A unifying model to explain high nirmatrelvir therapeutic efficacy, low post-exposure prophylaxis efficacy, and frequent viral rebound

Authors

Shadisadat Esmaeili,[1]*† Katherine Owens,[1†] Jessica Wagoner,[2] Stephen J. Polyak,[2] Judith M. White,[3] Joshua T. Schiffer[1,2]

Affiliations

[1]Vaccine and Infectious Disease Division, Fred Hutchinson Cancer Center; Seattle, WA, USA.

[2]Department of Medicine, University of Washington; Seattle, WA, USA.

[3]Department of Cell Biology, University of Virginia; Charlottesville, VA, USA.

*Corresponding Author: sesmaeil@fredhutch.org

† These authors contributed equally to this work.

Abstract

In a pivotal trial, a 5-day course of oral ritonavir-boosted nirmatrelvir, given early during symptomatic infection, decreased hospitalization and death by 89.1% and reduced nasal viral load by 0.87 log relative to placebo in high-risk individuals. Yet, ritonavir-boosted nirmatrelvir failed as post-exposure prophylaxis in a follow-up trial, and frequent viral rebound has been observed in the community. We developed a mathematical model capturing viral-immune dynamics and nirmatrelvir pharmacokinetics that recapitulated viral loads from this and another clinical trial. Our results suggest that nirmatrelvir's *in vivo* potency is significantly lower than *in vitro* assays predict. A maximally potent agent would reduce the viral load by approximately 3.5 logs relative to placebo at 5 days. The model identifies that earlier initiation and shorter treatment duration are key predictors of post-treatment rebound. Extension of early symptomatic treatment to 10 days and post-exposure prophylaxis to 15 days, rather than increasing dose or dosing frequency, is predicted to significantly lower the incidence of viral rebound.

Introduction

The SARS-CoV-2 main protease inhibitor nirmatrelvir is a drug plagued by contradictions. In a landmark, randomized, double-blinded, placebo-controlled clinical trial with 1364 analyzed individuals, 300 mg of nirmatrelvir boosted with 100 mg ritonavir was given twice daily for five days to high-risk individuals with SARS-CoV-2 infection within 3 days of developing symptoms. Compared to placebo, nirmatrelvir reduced the combined outcome of hospitalization and death by 89%, eliminated death as an outcome, and reduced viral load by 0.87 log after 5 days of treatment*(1)*. This critical result prompted the Food and Drug Administration (FDA) to issue an Emergency Use Authorization*(2)*. The drug became the most widely prescribed antiviral for SARS-CoV-2 in the United States, likely preventing thousands of hospitalizations and many deaths*(3)*. Ritonavir boosted nirmatrelvir was recently licensed by the FDA based on its continued effectiveness and safety*(4)* and has outperformed other antivirals in terms of hospitalization and viral load reduction*(5)*.

However, the use of nirmatrelvir/ritonavir in real-world cohorts has identified viral rebound as a significant issue. Viral rebound occurred in 14.2% of individuals in one large cohort and was usually associated with recrudescence of symptoms, though protection against hospitalization and death appeared to be maintained*(6)* and remains significant despite high rates of population immunity due to vaccination and prior infection*(7)*. Similar rates of viral rebound were observed between molnupiravir and nirmatrelvir, suggesting the rebound effect is not drug-specific and may pertain to characteristics of SARS-CoV-2 infection and treatment duration*(8)*. This high incidence of viral rebound exceeded the 2.3% rate observed in the proof-of-concept trial, which did not differ from placebo*(9)*.

Despite its high efficacy as an early symptomatic therapy for high-risk individuals, nirmatrelvir/ritonavir was not authorized for use as post-exposure prophylaxis (PEP). In a clinical trial of post-exposure prophylaxis, nirmatrelvir/ritonavir showed 32% and 37% reductions in symptomatic COVID-19 relative to placebo when given for five or ten days respectively*(10)*. However, neither of these results reached statistical significance. Notably, molnupiravir, another drug that reduced hospitalization when given during early symptomatic infection, also failed as post-exposure prophylaxis*(11)*. Only long-acting monoclonal antibodies have demonstrated efficacy for post-exposure prophylaxis*(12–14)*, but these are no longer active against prevalent circulating strains*(15)*.

Early during the COVID-19 pandemic, multiple groups employed mathematical models to predict the outcomes of clinical trials for SARS-CoV-2*(16–22)*. These models all accurately predicted that antiviral therapy that was insufficiently potent or given too late during infection might fail to provide clinical benefit*(16–19, 21)*. Our previous modeling results further suggested that viral rebound may occur and was more likely if a drug was dosed during the pre-symptomatic phase of infection when viral loads are still expanding, as occurs in a post-exposure prophylaxis scenario*(23)*. The proposed mechanism of this effect was that reducing viral load may blunt early immune responses and preserve susceptible cells, allowing viral re-expansion upon cessation of treatment that was of insufficient potency to eliminate all infected cells*(24)*. The model suggested that this phenomenon could theoretically occur during early symptomatic treatment as well. At the time, we downplayed the significance of model-generated rebound as the phenomenon had yet to be demonstrated clinically. However, models fit to rebound data now suggest a similar mechanism of action to explain viral rebound*(25)*.

Here we use an updated model for SARS CoV-2 viral kinetics that was first validated against a much larger panel of untreated individuals to precisely simulate the virologic outcomes of two nirmatrelvir/ritonavir trials. We identify that the true *in vivo* potency of nirmatrelvir is approximately significantly less than its *in vitro* potency, such that drug levels are sub-therapeutic during a portion of the dosing interval. Viral rebound is observed in our simulations and is more likely when the drug is dosed early during infection and is not reduced with a higher dose or dosing frequency. Extended-duration treatment is identified as the best strategy to avoid viral rebound.

Results

Viral Dynamic, Pharmacokinetic, and Pharmacodynamic Mathematical models

To derive parameters for simulating nasal viral loads in the absence of therapy, we used the mechanistic mathematical model that best recapitulated 1510 SARS-CoV-2 infections in a cohort of 2678 SARS-CoV-2 infected individuals from the National Basketball Association cohort (Error! Reference source not found.**a**) *(26)*. The model is target-cell limited due to a finite number of susceptible cells. An eclipse phase delays viral production by infected cells. In keeping with an early interferon-mediated innate immune response, susceptible cells can become refractory to infection based on the total number of productively infected cells but also revert to susceptible at a constant rate. Infected cells are cleared by cytolysis and early immune response at a constant rate and delayed acquired immunity, which is activated in a time-dependent fashion. We used a mixed-effect population approach implemented in Monolix to estimate model parameters **(Fig S1, Table S1)**.

To reproduce levels of nirmatrelvir, we used a two-compartment pharmacokinetic (PK) model (Error! Reference source not found.**b**). Using Monolix and the mixed-effect population approach, we estimated parameter values by fitting the model to the plasma concentration of healthy subjects. The model closely recapitulated observed drug levels following a single dose of 250mg/100mg of nirmatrelvir/ritonavir **(Fig S2, Table S2)**. The effect of ritonavir as an inhibitor of nirmatrelvir's metabolism is accounted for in the nirmatrelvir's clearance rate in the PK model. We also fit the model to the population level plasma concentrations following a single dose of 250mg/100mg and 750mg/100mg showing that the estimated parameters are dose-independent **(Table S3).**

For the pharmacodynamic (PD) model, we assumed the efficacy of the drug follows a Hill equation with respect to the drug concentration. We parameterized the Hill equation using *in vitro* efficacy data collected at different concentrations of nirmatrelvir (details in **Materials and Methods, Fig S3, Table S4**).

To estimate the *in vivo* potency of nirmatrelvir/ritonavir, we fit our model to the viral load drop from the baseline of the control and treatment arms of two randomized, controlled trials: the EPIC-HR trial with 1574 high-risk unvaccinated symptomatic individuals (trial 1)*(1)*and the PLATCOV trial with 144 low-risk, symptomatic individuals (trial 2) *(5)*. To generate placebo arms for each trial with matched viral variants and vaccine status, we simulated the viral load of 400 randomly selected individuals from the unvaccinated symptomatic subgroup of the NBA cohort (for EPIC-HR) and symptomatic individuals with Omicron infection (for PLATCOV), using their estimated individual viral load parameters. For their symptom onset, we randomly assigned all individuals an incubation period selected from a gamma distribution with parameters associated with each participant's variant reported in the

literature *(27)*. The mean viral load drop from the baseline recapitulated the mean change from the baseline of the viral load observed in the control arms of both trials (Error! Reference source not found.**a and 3a**).

To simulate the treatment arm, we combined viral dynamics, PK, and PD models. Sets of VL parameters for individuals were again drawn from the NBA cohort following the same criteria as in the control arm to match the cohort characteristics of each trial as closely as possible. The PK and PD parameters for all simulated individuals were randomly drawn from their estimated population distributions. The efficacy of the treatment was calculated from the Hill equation using plasma concentrations of the drug obtained from the PK model. The efficacy of the treatment was used to lower the viral reproduction rate (details in **Materials and Methods, Fig 1**).

Reduction of *in vivo* nirmatrelvir potency relative to *in vitro*

To obtain PD parameters of nirmatrelvir, we fit the Hill equation to the *in vitro* efficacy of the drug as a function of its concentration (**Fig S3**). However, the *in vivo* potency of a drug is known to be different from values measured *in vitro(23, 28, 29)*. The potency reduction factor (prf) is defined as the ratio between the *in vivo* and *in vitro* IC_{50}. Here the *in vivo* IC_{50} is the plasma drug concentration required to inhibit viral replication by 50%. To identify the *in vivo* potency of nirmatrelvir, we estimated the prf that achieved the best fit between our VL+PKPD model and the average drop in viral load of the treatment arm of the two clinical trials (**Figs 2b and 3b**).

To estimate the prf, we simulated the viral load of our virtual cohort of 400 individuals treated with 300 mg of nirmatrelvir twice per day for five days with prf ranging from 1 (no reduction in potency) to 120. The treatment start day was randomly selected from a uniform distribution for each simulated individual to be within 3 days of symptom onset. We fit the average change from baseline in simulated viral load data of the treatment arm to the trial data. We then plotted the coefficient of determination, R^2, of the fit against different prf values (**Figs 2c and 3c**). The best value (prf = 61 for the fit to EPIC-HR and prf=37 when fitting to PLATCOV) was determined by maximizing the R^2 of the fit. Our model closely recapitulated viral load reduction in the treatment arm of both trials (**Figs 2b and 3b**). We repeated the simulation 10 times and used these replicates to estimate the standard error of the prf. Accordingly, the boxplot in the lower panel of **Figs 2c** and **3c** represents the standard error of the prf average value and does not reflect individual variability.

The reason for slight differences in estimated prfs between the two trials is unknown. Possible explanations include different sampling methods (nasal swabs in EPIC-HR versus oropharyngeal swabs in PLATCOV) or different participant characteristics (high-risk adults in EPIC-HR versus lower-risk adults without comorbidities in PLATCOV).

Estimates of optimal viral load reduction with an optimal drug

To illustrate the importance of estimating *in vivo* potency of the drug, we compared the PKPD projection and average change in viral load of treatment arms with prf = 1 (no reduction in potency) and prf = 61. With an approximately 61-fold weaker potency, the drug levels dropped below the therapeutic level shortly after each dose and antiviral effect subsided in less than a day after the end of treatment leading to an average efficacy of 82% over the first 5 days of treatment (**Fig 2d, e**). However, the plasma concentration of a perfectly potent drug (prf = 1) remained above therapeutic levels for the duration of the treatment with a 5-day average efficacy of 99.99% and the effect

persisted for nearly 10 days (**Fig 2e**). With the perfectly potent drug (prf =1), with assumed *in vitro* potency level, the same treatment regimen could reduce the viral load by approximately 3.5 logs at day 5 relative to the placebo compared to the 0.87 log reduction reported in the trial (**Fig 2f**).

In estimating nirmatrelvir's *in vitro* pharmacodynamic parameters, we assumed only the IC_{50} differs *in vivo*. To confirm the validity of this assumption, we repeated the simulation of the treatment arm of EPIC-HR with different combinations of the potency reduction factor and the Hill coefficient. **Fig S4** shows that the best fit always happened for prf ~60 and was independent of the Hill coefficient.

The potency reduction factor was more sensitive to certain PK parameters **(Fig S5),** particularly the drug's clearance rate (κ_{CL}). If the drug is assumed to be cleared from the body more rapidly (larger κ_{CL}), then it would need to be more potent (smaller prf) to provide the same effect observed in the clinical trial. However, this did not impact our simulations of different dosing regimens since PK parameters were independent of the dose **(Table S3)**. In simulations of different dosing regimens, we therefore use estimated PK parameters and prf distributions from EPIC-HR for all dosing regimens.

Model recapitulation of PLATCOV participant variability

Our model accurately reproduced mean reduction in viral load on multiple post-treatment days in EPIC-HR **(Fig 2b)** and PLATCOV **(Fig 3b)**. However, it also predicted variable virologic responses at the individual level, including some instances of viral increase in the days following therapy. To test whether our model reproduced individual level heterogeneity within the trial, we compared simulated and actual distributions of viral load change in the control and treatment arms of the PLATCOV trial. On most post-treatment days, these distributions were not statistically dissimilar (**Fig 3d, e**). Wider distributions of observed versus simulated viral load change were noted on post-randomization days 1 and 2 in the control and days 1 and 4 in the treatment arm (**Fig 3d, e**) perhaps due to noise in viral load data from oral swabs: wide variability was noted between oral samples collected from PLATCOV participants at equivalent timepoints, particularly on day 1 and 2 (**Fig S6**).

Frequent viral rebound on nirmatrelvir

To assess whether our model generated viral rebound, we performed simulations assuming parameter values obtained from fitting the model to data from the EPIC-HR trial **(Fig 2)** and randomly drew individual prf values from the obtained distribution in **Fig 2c**. We performed simulations from the time of infection to 30 days after symptom onset and monitored viral load continually. We defined rebound in the control arm as any case with at least two peaks in the viral load trajectory with minimum heights of 3 logs and a second peak higher than its minimum by at least 1 log **(Fig S7a)**. We defined rebound in the treatment arm as any instance in which a post-treatment viral load exceeded the viral load at the end of the treatment by 1 log **(Fig S7b)**.

By this definition, we observed rebound in 21.6% of cases treated with the clinical trial dose and 3.78% of controls **(Fig 4b)**. When an equivalent definition of rebound was used as in the trial (1 log increase in viral load 5 days after treatment cessation), the probability of rebound was lower (6.65% if treatment was assumed to begin several days after symptoms), closer to that of the controls, and comparable to that observed in the trial **(Fig S8).**

Limited impact of nirmatrelvir dose or dosing frequency on viral rebound

We next explored different treatment regimens to estimate their impact on lowering viral load and the chance of rebound. We simulated the therapy with 150, 300, 600, and 900 mg doses administered twice per day for 5 days, starting within 3 days post symptom onset. A larger dose decreased viral load more significantly and quickly than 300 mg twice daily. 900 mg of nirmatrelvir reduced the viral load by a mean of 2 logs on day 2 and a mean of 4 logs on day 5 compared to the control (**Fig 4a**).

Individual viral loads were highly variable within each treatment group regardless of dose **(Fig 4a)**. This was due to several factors including heterogeneous viral load trajectories **(Fig S1)** and different timing of treatment. Responses to treatment differed substantially according to viral load trajectory and treatment timing as well **(Fig 4c).** In nearly every case, the reduction in viral load was greater during the first 5 days of treatment with higher doses. However, this only impacted viral elimination in certain cases (**Fig 4c,i)**. Sometimes viral load equilibrated to similar levels post-treatment regardless of dose **(Fig 4c, ii)**, while in other cases, higher doses were associated with rebound **(Fig 4c, iii & iv)**. By achieving a lower post-treatment viral load nadir, higher doses resulted in a greater likelihood of viral rebound in our simulations **(Fig 4b)**.

Increasing frequency of antiviral dosing had nearly equivalent effects to increasing the dose, leading to a more rapid reduction in viral load **(Fig S9a)**, heterogeneous effects based on viral load trajectory and timing of treatment **(Fig S9c)**, and increased chance of rebound **(Fig S9b)**.

Early treatment as a predictor of SARS-CoV-2 rebound

We next simulated therapy with four different timings of treatment: post-exposure prophylaxis (PEP): 0-1 day after infection in the pre-symptomatic phase; early treatment: 0-1 day after symptom onset as often occurs in community settings; intermediate treatment: 1-5 days after symptom onset as in the clinical trial; and late treatment: 5-10 days after symptom onset. In all simulations, the administered dosage was 300mg twice per day for 5 days.

Applying treatment as PEP or shortly after symptoms lowered viral load more substantially relative to control than intermediate or late therapy at days 2 and 5 post-treatment, though intermediate and late strategies also significantly lowered viral load relative to control at these timepoints **(Fig 5a)**. The boxplots for control groups in each panel in **Fig 5a** show the viral load at different points during the infection to match different timing of the treatment in the treatment arms. However, mean viral load was significantly higher in the PEP group versus the control group 10 days after the start of treatment (**Fig 5a**), due to the high probability of rebound **(Fig 5b, c)** when the virus is at its initial stages of expanding in the body and before the immune response is established in treated individuals.

Prolongation of treatment to reduce the probability of SARS-CoV-2 rebound

Next, we analyzed the impact of treatment duration on viral rebound. We simulated treatment regimens with 300 mg nirmatrelvir given twice per day for 2, 5, 10, 15, and 20 days. The treatment was again initiated within 3 days after symptoms appeared. **Fig 6a** demonstrates the continuous drop in viral load if treatment was maintained until the infection was effectively cleared from the body. The viral load distributions of the treatment arms with 15 and 20 days of treatment on days 2, 5, and 10 were the same as the viral load distribution of the treatment arm with 10 days of treatment duration and, therefore, are not shown. Prolonging treatment duration to 20 days almost completely eliminated viral rebound (**Fig 6b,c**).

We next explored the impact of treatment duration on different treatment timing. Prolonging treatment to 15 days for early treatment and 20 days for PEP lowered the viral load close to the limit of detection (2 log) at the end of treatment and significantly lowered the probability of rebound (**Fig 7**).

Differing observed rebound rates resulting from varying timing of sampling and definitions

Previous studies have defined rebound using criteria with varying virologic thresholds, timing, and sampling frequency *(30)*. A rebound was sometimes defined when a positive test was observed after a negative test *(31)*. In EPIC-HR, treatment was started within the first 5 days of symptoms (our intermediate treatment group) and rebound was defined as a 0.5 log increase on days 10 and/or 14. By this definition 2.3% of treated cases were classified as rebound *(30)*. The probability of rebound in our simulation with a threshold of 0.5 log measured only on day 5 after the end of the treatment was 8.15% and decreased as thresholds for viral rebound increased (**Fig S8**). This percentage would be even lower if treatment started 3-5 days after symptoms (rather than 1-5 days) because the probability of rebound is very sensitive to the timing of treatment. We hypothesize that in EPIC-HR, participant enrollments were skewed to later during the first 5 day symptom window.

In our simulations, we recorded viral load every 0.001 of a day and used a 1 log threshold to identify rebound cases. This would be a more sensitive method to observe rebound and suggests that in trial and real-world cohorts, rebound is likely more common in treated individuals than is detected with less frequent sampling (**Fig S8**).

Immune and viral mechanisms for viral rebound

To understand mechanisms that might explain the increase in rebound in the PEP and early treatment groups, we simulated four treatment arms with the treatment starting on days 1, 4, 7, and 10 after infection. The start day was fixed for all individuals in each arm to limit the added variability introduced by a variable incubation period and timing of treatment relative to symptoms in our previous simulations. The high frequency of rebound in day 1 and day 4 treatment starts was evident from the viral load trajectories after the end of the treatment on days 5 and 9, respectively (**Fig 8a** top row), in many individual trajectories (grey lines) and to a less dramatic extent in mean viral load (blue line). A second peak after the end of the treatment was also seen in the dynamics of infected cells (**Fig 8a** middle row, blue line) and the intensity of the innate immune response (the rate of production of refractory cells) (**Fig 8a** bottom row).

Applying the treatment earlier during infection (day 1 and day 4 in the case of our simulations) lowered the viral load as well as the populations of infected and refractory cells, preserving susceptible cells. The ratio of susceptible to refractory cells in the two groups with earlier treatment starting points (day 1 and day 4) was significantly higher at the end of the treatment than in the control group at equivalent time points (**Fig 8b)**. At each time point, innate immune responses were significantly diminished in treated individuals versus controls due to fewer infected cells **(Fig 8c)**. Overall, a weaker innate immune response, higher availability of susceptible cells and persistence of infected cells after 5 days of treatment, allowed viral rebound after treatment cessation.

In a parallel manuscript, we subset shedding groups in the NBA cohort according to shedding kinetics using k-means clustering. The groups were ordered based on the area under their viral load curve (AUC) with group 1 having the smallest AUC and group 6 the largest (**Fig S10a**). We simulated treatment with different treatment start days using

these 6 groups and identified the highest rebound probability in the earlier treatment groups with the larger AUC (groups 5 and 6) and longer time to peak viral load (groups 3, 5, and 6) prior to antiviral therapy (**Fig S10b, c**). This indicates that viral rebound may be more likely in individuals who were destined for more severe infections had they not received therapy.

Discussion

We previously demonstrated for herpes simplex virus-2*(32)*, HIV*(33)*, Ebola virus*(28)*, and SARS-CoV-2*(23)*, that it is vital to consider the timing and intensity of the immune response to accurately simulate clinical trials of antiviral agents. If a direct-acting antiviral therapy is given too late during infection, then efficacy is often low because the disease is driven by excess inflammation and cytokine storm. On the other hand, concurrent immune pressure can provide critical assistance for antiviral agents to eliminate viral replication, as confirmed in recent studies*(7)*. Accordingly, our previous modeling suggested that extremely early treatment of pre-symptomatic SARS-CoV-2 as occurs with PEP requires higher drug potency than treatment during early symptomatic infection because innate immunity is activated to a greater extent at this slightly later stage of infection and fewer susceptible cells remain*(23)*. It is increasingly clear that the potency and duration of antiviral therapy required to achieve clinical benefit depends strongly on the stage of infection and the ongoing intensity of the immune response.

Our prior work also demonstrated that *in vitro* antiviral drug potency measured in relevant cell culture lines often overestimates *in vivo* potency in humans*(28, 29, 34)*. Specifically, the plasma drug level required to achieve 50% inhibition of cellular infections *in vivo* is higher than the level required to inhibit infection *in vitro*. The discrepancy between *in vitro* and *in vivo* potency can only be assessed by fitting viral dynamic / PKPD mathematical models to viral load data from clinical trials, as we have done here. Traditional PKPD models, which do not account for the dynamics of an immune response on observed viral loads, are not sufficient to estimate *in vivo* potency. Because *in vivo* potency reduction varies from 2 to 100 depending on the infection, antiviral agents*(28, 32, 34)*, and population *in vivo* IC_{50} must be assessed separately in each case.

Here by precisely fitting a combined viral-immune dynamic / PKPD model to viral load data from placebo and treatment groups in a randomized clinical trial as well as an open-label clinical trial of nirmatrelvir/ritonavir, we merge these two key concepts. We first identify that nirmatrelvir potency is reduced 60-70 fold *in vivo* relative to *in vitro* in the high-risk population and 30-40 fold in the healthy population. The difference between the estimated *in vivo* potency in these two populations can be explained by the differences in the demographics and sampling methods in the two trials. The mechanistic reasons for this reduction cannot be determined by the model but may include increased *in vivo* protein binding*(35)*, inhibition of drug delivery from plasma to sites of infection, or differences in cellular uptake and drug metabolism *in vivo(36)*. Nevertheless, our estimated *in vivo* IC_{50} provides a benchmark plasma level to target in future trials. The PK model also demonstrates that the drug's relatively short half-life ($t_{½}$) allows it to dip to subtherapeutic levels even when dosed twice daily.

Our model also develops a viable hypothesis for why nirmatrelvir is highly effective when given during early symptomatic infection but less so when given as post-exposure prophylaxis. By preventing a high peak viral load approximately 3-5 days after infection, therapy preserves susceptible cells and blunts the immediate, likely innate

immune response to SARS-CoV-2, while not completely eliminating infected cells. If the virus is not eliminated by an early acquired response along with antiviral pressure, it rebounds to a peak level that is sometimes comparable to the initial peak. We hypothesize that viral rebound occurs more frequently in community settings relative to the clinical trial. Infected individuals in the community are often prescribed the drug very early after symptom development, whereas in the trial, there was a natural 1 to 2-day delay based on the enrollment and consent process. Surprisingly, this short delay may have limited rebound while not affecting the primary endpoints of the trial, a finding supported by recent clinical studies*(37)*, which nevertheless still suggest a clear benefit for earlier treatment in terms of preventing hospitalization in high-risk individuals*(7)*. Notably, antiviral therapy is not a risk factor for rebound in our model or in clinical cohorts of individuals treated late during infection*(38)*. High viral load shedding is also a risk factor for rebound in our model as has been suggested in other studies *(39)*.

Our model identifies optimal conditions for viral rebound, which counterintuitively include early treatment during pre-symptomatic infection, which can be exacerbated by higher or more frequent dosing. Both mechanisms occur by suppressing the amount of infection and preserving susceptible cells, limiting the development of refractory cells, and dampening the intensity of the early immune response. The best method to prevent viral rebound is prolonging treatment, with a longer course needed for PEP. This finding is consistent with trials of long-acting monoclonal antibodies, which demonstrated efficacy as post-exposure prophylaxis*(12–14)*.

Because the model is validated precisely against mean viral load reduction from two trials as well as individual viral kinetic distributions within each arm of one trial, it can be used as a tool to test various treatment strategies for future trials with the ability to vary therapeutic goals, timing of treatment, dose, dosing interval, and duration of therapy. Our prior PD modeling also allows testing of potentially synergistic combination agents and consideration of special hosts such as immunocompromised individuals with persistent infection who may be at risk of developing drug resistance*(28, 40)*. We believe our approach provides a template for optimizing future trial designs with nirmatrelvir and other therapies.

Our model has several limitations. First, nasal or oropharyngeal viral load may not be a perfect surrogate of disease activity. On the one hand, viral load reduction has been correlated with beneficial clinical outcomes for nirmatrelvir*(1)*, molnupiravir*(41)*, and monoclonal antibodies*(42)*. A recent review shows that viral load reduction is a reasonably good surrogate endpoint*(42)*. Moreover, the viral rebound appears to track very closely with the symptomatic rebound in multiple case series*(30)*. Yet, early remdesivir treatment provided a profound reduction in hospitalization while not impacting nasal viral load, albeit 5 days after completion of therapy *(43)*. Data from non-human primates suggests that the drug has a specific effect on viral loads in the lungs that is not observed in upper airways, a finding that we were also able to capture with models*(23)*. Overall, there is a strong suggestion from early treatment trials that a reduction in nasal viral loads beyond that observed in placebo-treated individuals is associated with substantial clinical benefit*(1)*.

Another limitation is that the model does not account for drug resistance. While there has been limited evidence of de novo resistance during nirmatrelvir therapy, serial passage of virus suggests a relatively low barrier, and some viral rebound could, in theory, be with resistant variants. Studies to date suggest very little mutational change between the infecting and rebounding virus*(44–47)*.

Our model does not capture immunity in literal terms. For instance, we do not distinguish innate interferon, antibody, and T-cell responses, as these have not been measured in sufficient longitudinal detail to precisely ascribe viral clearance to different components of the immune response. We structured the model for the early response to roughly map to innate responses, as the model term capturing the progression of susceptible cells to a refractory state diminishes with decreases in viral load and assumes no immune memory. The late immune response in our model has memory, leads to rapid elimination of the virus, and is likely to represent acquired immunity. While a more accurate model would discriminate different arms of the immune responses and fit to immune data, ours sufficiently captures the timing and intensity of immune responses for accurate clinical trial simulation.

Finally, it is our opinion that models lacking a spatial component cannot capture the full dynamics of target cell limitation, which is influenced by the packing structure of cells, dynamics of viral diffusion, and infection within multiple concurrent micro-environments*(32)*. For these reasons, ordinary differential equations may misclassify the relative impact of target cell limitation and innate immune responses in the period surrounding peak viral load. However, our differential equation approach provides accurate output for clinical trial simulation.

In conclusion, our model identifies viable mechanistic underpinnings of the high efficacy of nirmatrelvir therapy for early symptomatic SARS-CoV-2 infection, lower efficacy for PEP, and high incidence of viral rebound in a real-world setting. The model can also be used to assess different treatment strategies and suggests prolonging therapy is the optimal method to avoid rebound and maintain potent early antiviral suppression.

Materials and Methods

Study Design

We developed a viral dynamics model recapitulating the viral load data collected from symptomatic individuals in the NBA (National Basketball Association) cohort*(48)*. We used a two-compartment model to reproduce the PK data of nirmatrelvir plus ritonavir*(2)*. For the simulation, we constructed a virtual cohort by randomly selecting 400 individuals from the NBA cohort, trying to match the trial populations regarding the vaccine status and history of infection, and assigning individual PK and PD parameters randomly drawn from their respective inferred distributions. We fit the combined viral dynamics and PK/PD model to the average change in viral load from the baseline of the control and treatment arms of the two previously published nirmatrelvir/ritonavir clinical trials *(1, 5)*. By fitting our model to the control arms, we validated our viral dynamics model and how well the viral dynamics of our virtual cohort represent the trial control arms. We used the fit to the treatment arms to estimate the potency reduction factor (prf) by maximizing the R^2 of the fit. With the estimated prf and *in vivo* IC_{50} of the drug, we explored different treatment regimens by changing dose, dosing frequency, treatment duration, and treatment timing, to find the best strategy to minimize the probability of rebound.

Viral load data

We used data from the symptomatic subpopulation of the NBA cohort published by Hay et al*(48)*. The NBA cohort dataset consists of 2875 documented SARS-CoV-2 infections in 2678 people detected through frequent PCR testing regardless of symptoms. 1510 infections in 1440 individuals had at least 4 positive quantitative

samples. We used the viral load data from the 1510 infections to estimate the viral load parameters.

Clinical trial data

We used viral load data from two nirmatrelvir/ritonavir clinical trials. EPIC-HR by Hammond et al. *(1)* included 682 and 697 symptomatic high-risk individuals in the control and treatment arms, respectively. We obtained the average change in viral load data of the control and treatment arms by digitizing Figure 3A of the manuscript*(1)*. Nasal viral load was measured on days 0, 3, 5, 10, and 14 after the treatment start day and adjusted by the baseline viral load. PLATCOV by Schilling et al. *(5)* is an open-label, randomized, controlled adaptive trial with 85 and 59 symptomatic, young, healthy individuals in the control and nirmatrelvir treatment arms, respectively. The viral load samples from each participant were collected on days 0 through 7 and day 14 after treatment start day. We used the individual viral load data made available by the authors. From PLATCOV, we averaged over the two oral samples collected from each individual and calculated viral load drop from baseline. In both trials, the study participants were treated with 300mg/100mg nirmatrelvir/ritonavir within three days (EPIC-HR) or four days (PLATCOV) of symptoms onset. The treatment was administered twice per day, for five days. We used EPIC-HR's lower limit of detection (2 log imputed as 1 log) in our simulations. However, when fitting to PLATCOV, we used the maximum LOD reported in the published data.

PK data

PK data of nirmatrelvir (PF-07321332) with ritonavir was obtained by digitizing Figure 4 of the drug's Emergency Use Authorization document*(2)*. The data is from a phase I randomized trial by Singh et al.*(49)* where eight participants (4 fed, 4 not fed) took a single dose of 250mg/100mg nirmatrelvir/ritonavir. The plasma concentrations of the drug in participants were recorded in the next 48 hours after dosing.

PD data

The data on drug efficacy comes from five replicates per condition, pooled from 2 independent technical experimental repeats (one experiment with triplicate conditions, one experiment in duplicate conditions) performed at the University of Washington. The efficacy of Nirmatrelvir in the presence of CP-100356 (an efflux inhibitor *(50)*) was measured against the delta variant of SARS-CoV2 in Calu-3 cells. The efflux inhibitor ensures consistent, adequate intracellular levels of drug. Briefly, Calu 3 cells human lung epithelial were treated with varying concentrations of nirmatrelvir in the presence of 2uM CP-100356 prior to infection with SARS-CoV-2 (delta isolate) at a multiplicity of infection of 0.01. Antiviral efficacy and cell viability (of non-infected cells treated with drugs) were assessed as described*(51)*.

Viral dynamics model

We used our model of SARS-CoV-2 dynamics*(26)* to model the viral load dynamics of symptomatic individuals with SARS-CoV-2 infection. Our model assumes that susceptible cells (S) are infected at rate βVS by SARS-CoV-2 virions. The infected cells go through a non-productive eclipse phase (I_E) before producing viruses and transition to becoming productively infected (I_P) at rate κI_E. When encountering productively infected cells, the susceptible cells become refractory to infection (R) at the rate $\phi I_P S$. Refractory cells revert to a susceptible state at rate ρR. The productively infected cells are cleared at rate δI representing cytolysis and the innate immune response that lacks memory and is proportional to the amount of ongoing infection. If

the infection persists longer than τ, then cytotoxic acquired immunity gets involved, which is represented in our model by the rate mI_P. Finally, free virions are cleared at the rate γ. Of note, this model, previously proposed by Ke et al. *(52)*, was selected against other models in*(26)* based on superior fit to data and parsimony. The model written as a set of differential equations has the form,

$$\frac{dS}{dt} = -\beta SV - \phi I_P S + \rho R \quad (1a)$$

$$\frac{dR}{dt} = \phi I_P S - \rho R \quad (1b)$$

$$\frac{dI_E}{dt} = \beta SV - \kappa I_E \quad (1c)$$

$$\frac{dI_P}{dt} = \kappa I_E - \delta I_P - m(t) I_P \quad (1d)$$

$$\frac{dV}{dt} = \pi I_P - \gamma V \quad (1e)$$

$$\text{where} \begin{cases} m(t) = 0 & t < \tau \\ m(t) = m & t \geq \tau \end{cases} \quad (1f)$$

To estimate parameter values, we fit the model to viral load data from the NBA cohort using a mixed-effect population approach implemented in Monolix.

We start the simulations with 10^7 susceptible cells. The initial value of the refractory cells is assumed to be zero since the interferon signaling is not active prior to infection. We further assume there are no infected cells (eclipse or productive) at the beginning of the infection. We fix the level of inoculum (V_0) at 97 copies/ml for each individual.

To resolve identifiability issues, we fixed two parameter values, setting the inverse of the eclipse phase duration to $\kappa = 4$, the rate of clearance of virions to $\gamma = 15$*(26)*.

PK model

We used a two-compartmental PK model which includes the amount of drug in the GI tract (A_{GI}), the plasma compartment (A_p), and the lung (A_L). The drug is administered orally, passes through the GI tract and gets absorbed into the blood at the rate κ_a. The drug then transfers from the blood into the peripheral compartment (or the lung) at the rate κ_{PL}. The metabolized drug transfers back into the plasma at the rate κ_{LP} from where it clears from the body at the rate κ_{CL}. The model in the form of ordinary differential equations is written as,

$$\frac{dA_{GI}}{dt} = -\kappa_a A_{GI} \quad (2a)$$

$$\frac{dA_P}{dt} = \kappa_a A_{GI} + \kappa_{LP} A_L - (\kappa_{CL} + \kappa_{PL}) A_P \quad (2b)$$

$$\frac{dA_L}{dt} = \kappa_{PL} A_P - \kappa_{LP} A_L \quad (2c)$$

We used Monolix and a mixed-effect population approach to estimate the parameters and their standard deviations. With the initial condition of ($A_{GI} = Dose$, $A_p = 0$,

$A_L = 0$); we fit $C_P = \frac{A_P}{Vol}$ to the plasma concentration data where Vol is the estimated plasma volume.

PD model

For the pharmacodynamics model we used Hill equation, $\epsilon(t) = \frac{E_{max} C(t)^n}{C(t)^n + IC_{50}^n}$, where $C(t)$ is the drug's concentration in plasma, E_{max} is the maximum efficacy, n is the hill coefficient, and IC_{50} is the drug concentration in plasma required to provide 50% efficacy. We used least-squared fitting to obtain the three parameters and their standard deviations. The average drug efficacy is measured using,

$$E_{ave} = \frac{1}{t_{start} - t_{end}} \int_{t_{start}}^{t_{end}} \epsilon(t) dt \qquad (3)$$

Where t_{start} and t_{end} are the treatment start day and end day respectively.

Combined PKPD and VL models

The plasma concentration of nirmatrelvir obtained from the PK model is used in the PD model to obtain time-dependent efficacy. $\epsilon(t)$, then, is used to reduce viral production rate, π, with the factor of $\big(1 - \epsilon(t)\big)$. Equation 1e is written as,

$$\frac{dV}{dt} = \big(1 - \epsilon(t)\big)\pi I_P - \gamma V \qquad (4)$$

Construction of a virtual cohort

To generate a cohort for our simulated clinical trials, we randomly selected 400 individuals (for each arm of the simulated trial) from the unvaccinated symptomatic subpopulation of the NBA cohort and used their individual viral load parameters estimated by fitting our viral dynamics model to the data. For their incubation period, we drew randomly from gamma distributions with parameters associated with their variants of concern *(27)*. PK parameters of each simulated individual were randomly drawn from the lognormal distributions with their estimated mean and standard deviation inferred from PK data. The PD parameters were also randomly drawn from the normal distribution with the estimated mean and standard deviation. The standard deviation of the PD parameters represents the accuracy of the assays and not the individual variability. The individual potency reduction factors were also drawn from a normal distribution with mean and standard deviation obtained from fitting ten simulations to the treatment arm of trial 1.

Potency reduction factor (prf)

The potency reduction factor (prf) is defined as,

$$prf = \frac{IC_{50,in\ vivo}}{IC_{50,in\ vitro}} \qquad (5)$$

We estimated the prf by maximizing R^2 when fitting the change in viral load of the treatment arm of our simulation to the data from the treatment arm of the clinical trial.

Measuring rebound probability

A viral load rebound in the treatment arm was defined when the viral load at any time after treatment ended exceeded the viral load at the end of the treatment by 1 log. In the control group, viral rebound was defined in patients who had at least two peaks with maximum height of 1000 copies/ml in their viral load trajectories and the second peak was 1log higher than its local minimum **(Fig S7)**.

References

1. J. Hammond, H. Leister-Tebbe, A. Gardner, P. Abreu, W. Bao, W. Wisemandle, M. Baniecki, V. M. , Hendrick, B. Damle, A. Simon-Campos, R. Pypstra, J. M. Rusnak, Oral Nirmatrelvir for High-Risk, Nonhospitalized Adults with Covid-19. *N Engl J Med* **386**, 1397–1408 (2022).
2. Emergency Use Authorization for Paxlovid (nirmatrelvir tablets co-packaged with ritonavir tablets) Center for Drug Evaluation and Research (CDER) Review. *Foods and Drug Administration* (2021) (available at https://www.fda.gov/media/155194/download).
3. M. Khunte, S. Kumar, J. A. Salomon, A. Bilinski, Projected COVID-19 Mortality Reduction From Paxlovid Rollout. *JAMA Health Forum* **4**, E230046 (2023).
4. FDA Approves First Oral Antiviral for Treatment of COVID-19 in Adults. *Foods and Drug Administration* (available at https://www.fda.gov/news-events/press-announcements/fda-approves-first-oral-antiviral-treatment-covid-19-adults).
5. W. H. K. Schilling, P. Jittamala, J. A. Watson, S. Boyd, V. Luvira, T. Siripoon, T. Ngamprasertchai, E. M. Batty, C. Cruz, J. J. Callery, S. Singh, M. Saroj, V. Kruabkontho, T. Ngernseng, N. Tanglakmankhong, J. Tubprasert, M. Y. Abdad, W. Madmanee, J. Kouhathong, K. Suwannasin, W. Pagornrat, N. Piaraksa, P. Hanboonkunupakarn, B. Hanboonkunupakarn, K. Poovorawan, M. Potaporn, A. Srisubat, B. Loharjun, W. R. J. Taylor, V. Chotivanich, K. Chotivanich, M. Imwong, S. Pukrittayakamee, A. M. Dondorp, N. P. J. Day, M. M. Teixeira, W. Piyaphanee, W. Phumratanaprapin, N. J. White, N. J. White, W. H. Schilling, W. Phumratanaprapin, V. Luvira, J. J. Callery, N. P. Day, S. Pukrittayakamee, S. Boyd, C. Cruz, A. M. Dondorp, W. R. Taylor, J. A. Watson, W. Piyaphanee, K. Poovorawan, T. Ngamprasertchai, T. Siripoon, B. Hanboonkunupakarn, K. Chotivanich, P. Jittamala, M. Imwong, J. Thaipadungpanit, M. Ekkapongpisit, V. Kruabkontho, T. Ngernseng, J. Tubprasert, M. Y. Abdad, E. M. Batty, S. Singh, V. Chotivanich, W. Ruksakul, C. Sangketchon, P. Hanboonkunupakarn, S. Sookprome, M. Teixeira, P. J. Almeida, R. S. Aguiar, F. Santos, E. Ashley, M. Vongsouvath, K. Phommasone, A. Dubot-Pérès, S. Vidhamaly, A. Chingsanoon, S. Bisayher, D. Chommanam, T. J. Evans, V. Vidhamaly, L. Boutthasavong, M. Mayxay, M. Potaporn, A. Srisubat, B. Loharjun, Antiviral efficacy of molnupiravir versus ritonavir-boosted nirmatrelvir in patients with early symptomatic COVID-19 (PLATCOV): an open-label, phase 2, randomised, controlled, adaptive trial. *Lancet Infect Dis* **0** (2023), doi:10.1016/S1473-3099(23)00493-0.
6. J. A. Pandit, J. M. Radin, D. C. Chiang, E. G. Spencer, J. B. Pawelek, M. Diwan, L. Roumani, M. J. Mina, The Coronavirus Disease 2019 Rebound Study: A Prospective Cohort Study to Evaluate Viral and Symptom Rebound Differences in Participants Treated With Nirmatrelvir Plus Ritonavir Versus Untreated Controls. *Clinical Infectious Diseases* **77**, 25–31 (2023).
7. C. K. H. Wong, J. J. Lau, I. C. H. Au, K. T. K. Lau, I. F. N. Hung, M. Peiris, G. M. Leung, J. T. Wu, Optimal timing of nirmatrelvir/ritonavir treatment after COVID-19 symptom onset or diagnosis: target trial emulation. *Nat Commun* **14** (2023), doi:10.1038/s41467-023-43706-0.
8. L. Wang, N. A. Berger, P. B. Davis, D. C. Kaelber, N. D. Volkow, R. Xu, COVID-19 rebound after Paxlovid and Molnupiravir during January-June 2022. *medRxiv* (2022), doi:10.1101/2022.06.21.22276724.
9. A. S. Anderson, P. Caubel, J. M. Rusnak, Nirmatrelvir–Ritonavir and Viral Load Rebound in Covid-19. *New England Journal of Medicine* **387**, 1047–1049 (2022).
10. Pfizer Shares Top-Line Results from Phase 2/3 EPIC-PEP Study of PAXLOVID™ for Post-Exposure Prophylactic Use. *Pfizer* (available at https://www.pfizer.com/news/press-release/press-release-detail/pfizer-shares-top-line-results-phase-23-epic-pep-study).
11. Merck Provides Update on Phase 3 MOVe-AHEAD Trial Evaluating LAGEVRIO™ (molnupiravir) for Post-exposure Prophylaxis for Prevention of COVID-19 - Merck.com (available at https://www.merck.com/news/merck-provides-update-on-phase-3-move-ahead-trial-evaluating-lagevrio-molnupiravir-for-post-exposure-prophylaxis-for-prevention-of-covid-19/).
12. C. Hirsch, Y. S. Park, V. Piechotta, K. L. Chai, L. J. Estcourt, I. Monsef, S. Salomon, E. M. Wood, C. So-Osman, Z. McQuilten, C. D. Spinner, J. J. Malin, M. Stegemann, N. Skoetz, N. Kreuzberger, SARS-CoV-2-neutralising monoclonal antibodies to prevent COVID-19. *Cochrane Database Syst Rev* , Art. No.: CD014945 (2022).
13. M. P. O'Brien, E. Forleo-Neto, N. Sarkar, F. Isa, P. Hou, K. C. Chan, B. J. Musser, K. J. Bar, R. V. Barnabas, D. H. Barouch, M. S. Cohen, C. B. Hurt, D. R. Burwen, M. A. Marovich, E. R. Brown, I. Heirman, J. D. Davis, K.

C. Turner, D. Ramesh, A. Mahmood, A. T. Hooper, J. D. Hamilton, Y. Kim, L. A. Purcell, A. Baum, C. A. Kyratsous, J. Krainson, R. Perez-Perez, R. Mohseni, B. Kowal, A. T. Dicioccio, G. P. Geba, N. Stahl, L. Lipsich, N. Braunstein, G. Herman, G. D. Yancopoulos, D. M. Weinreich, Effect of Subcutaneous Casirivimab and Imdevimab Antibody Combination vs Placebo on Development of Symptomatic COVID-19 in Early Asymptomatic SARS-CoV-2 Infection: A Randomized Clinical Trial. *JAMA* **327**, 432–441 (2022).

14. M. P. O'Brien, E. Forleo-Neto, B. J. Musser, F. Isa, K.-C. Chan, N. Sarkar, K. J. Bar, R. V. Barnabas, D. H. Barouch, M. S. Cohen, C. B. Hurt, D. R. Burwen, M. A. Marovich, P. Hou, I. Heirman, J. D. Davis, K. C. Turner, D. Ramesh, A. Mahmood, A. T. Hooper, J. D. Hamilton, Y. Kim, L. A. Purcell, A. Baum, C. A. Kyratsous, J. Krainson, R. Perez-Perez, R. Mohseni, B. Kowal, A. T. DiCioccio, N. Stahl, L. Lipsich, N. Braunstein, G. Herman, G. D. Yancopoulos, D. M. Weinreich, Subcutaneous REGEN-COV Antibody Combination to Prevent Covid-19. *N Engl J Med* **385**, 1184–1195 (2021).

15. G. A. Herman, M. P. O'Brien, E. Forleo-Neto, N. Sarkar, F. Isa, P. Hou, K. C. Chan, K. J. Bar, R. V. Barnabas, D. H. Barouch, M. S. Cohen, C. B. Hurt, D. R. Burwen, M. A. Marovich, B. J. Musser, J. D. Davis, K. C. Turner, A. Mahmood, A. T. Hooper, J. D. Hamilton, J. Parrino, D. Subramaniam, A. Baum, C. A. Kyratsous, A. T. DiCioccio, N. Stahl, N. Braunstein, G. D. Yancopoulos, D. M. Weinreich, A. Chani, A. Adepoju, A. Mortagy, A. Dupljak, A. Brown, A. Froment, A. Hooper, A. Margiotta, A. Bombardier, A. Islam, A. Smith, A. Dhillon, A. McMillian, A. Breazna, A. Aslam, B. Carpentino, B. Kowal, B. Siliverstein, B. Horel, B. Zhu, B. Musser, B. Bush, B. Head, B. Snow, B. Zhu, C. Debray, C. Phillips, C. Simiele, C. Lee, C. Nienstedt, C. Trbovic, C. (Kuo C. Chan, C. Elliott, C. Fish, C. Ni, C. Polidori, C. Enciso, C. Caira, C. Powell, C. A. Kyratsous, C. Baum, C. McDonald, C. Leigh, C. Pan, D. Wolken, D. Manganello, D. Liu, D. Stein, D. M. Weinreich, D. Hassan, D. Gulabani, D. Fix, D. Leonard, D. Sarda, D. Bonhomme, D. Kennedy, D. Darcy, D. Barron, D. Hughes, D. Rofail, D. Kaur, D. Ramesh, D. Bianco, D. Cohen, E. Jean-Baptiste, E. Bukhari, E. Doyle, E. Bucknam, E. Labriola-Tomkins, E. Nanna, E. Huffman O'Keefe, E. Gasparino, E. Fung, F. Y. To, G. Herman, G. D. Yancopoulos, G. Bellingham, G. Sumner, G. Moggan, G. Power, H. Zeng, H. Mariveles, H. Gonzalez, H. Kang, H. Noor, I. Minns, I. Heirman, I. Peszek, J. Donohue, J. Rusconi, J. Austin, J. Yo, J. McDonnell, J. D. Hamilton, J. Boarder, J. Wei, J. Yu, J. Malia, J. Tucciarone, J. Tyler-Gale, J. D. Davis, J. Strein, J. Cohen, J. Meyer, J. Ursino, J. Im, J. Tramaglini, J. Wolken, K. Potter, K. Scacalossi, K. Naidu, K. Browning, K. Rutkowski, K. Yau, K. Woloshin, K. Lewis-Amezcua, K. Turner, K. Dornheim, K. Chiu, K. Mohan, K. McGuire, K. Macci, K. Ringleben, K. Mohammadi, K. Foster, L. Knighton, L. Lipsich, L. Darling, L. Boersma, L. Cowen, L. Hersh, L. Jackson, L. Purcell, L. Sherpinsky, L. Lai, L. Faria, L. Geissler, L. Boppert, L. Fiske, M. Dickens, M. Mancini, M. C. Leigh, M. P. O'Brien, M. Batchelder, M. Klinger, M. Partridge, M. Tarabocchia, M. Wong, M. Rodriguez, M. Albizem, M. O'Byrne, N. Deitz, N. Memblatt, N. Shah, N. Kumar, O. Herrera, O. Adedoyin, O. Yellin, P. Snodgrass, P. Floody, P. D'Ambrosio, P. (Xiaobang) Gao, P. Hearld, Q. Li, R. Kitchenoff, R. Ali, R. Iyer, R. Chava, R. Alaj, R. Pedraza, R. Hamlin, R. Hosain, R. Gorawala, R. White, R. Yu, R. Fogarty, S. B. Dass, S. Bollini, S. Ganguly, S. DeCicco, S. Patel, S. Cassimaty, S. Somersan-Karakaya, S. McCarthy, S. Henkel, S. Ali, S. Geila Shapiro, S. Kim, S. Nossoughi, S. Bisulco, S. Elkin, S. Long, S. Sivapalasingam, S. Irvin, S. Wilt, T. Min, T. Constant, T. Devins, T. DiCioccio, T. Norton, T. Bernardo, T. C. Chuang, V. (Jianguo) Wei, V. Nuce, V. Battini, W. Caldwell, X. Gao, X. Chen, Y. Tian, Y. Khan, Y. Zhao, Y. Kim, B. Dye, C. B. Hurt, D. R. Burwen, D. Burns, E. Brown, K. J. Bar, M. Marovich, M. Clement, M. S. Cohen, N. Sista, R. V. Barnabas, S. Zwerski, Efficacy and safety of a single dose of casirivimab and imdevimab for the prevention of COVID-19 over an 8-month period: a randomised, double-blind, placebo-controlled trial. *Lancet Infect Dis* **22**, 1444–1454 (2022).

16. K. Su, K. Ejima, Shoya Iwanami, Y. Fujita, H. Ohashi, Y. Koizumi, Y. Asai, S. Nakaoka, K. Watashi, K. Aihara, R. N. Thompson Id, R. Ke, A. S. Perelson, Shingo Iwami, A quantitative model used to compare within-host SARS-CoV-2, MERS-CoV, and SARS-CoV dynamics provides insights into the pathogenesis and treatment of SARS-CoV-2. *PLoS Biol* **19**, e3001128 (2021).

17. S. Wang, Y. Pan, Q. Wang, H. Miao, A. N. Brown, L. Rong, Modeling the viral dynamics of SARS-CoV-2 infection. *Math Biosci* **328**, 108438 (2020).

18. A. S. Perelson, R. Ke, Mechanistic Modeling of SARS-CoV-2 and Other Infectious Diseases and the Effects of Therapeutics. *Clin Pharmacol Ther* **109**, 829–840 (2021).

19. S. Sanche, T. Cassidy, P. Chu, A. S. Perelson, R. M. Ribeiro, R. Ke, A simple model of COVID-19 explains disease severity and the effect of treatments. *Sci Rep* **12**, 14210 (2022).

20. P. Czuppon, F. Débarre, A. Gonçalves, O. Tenaillon, A. S. Perelson, J. Guedj, F. Blanquart, Success of prophylactic antiviral therapy for SARS-CoV-2: Predicted critical efficacies and impact of different drug-specific mechanisms of action. *PLoS Comput Biol* **17**, e1008752 (2021).

21. A. Gonçalves, J. Bertrand, R. Ke, E. Comets, X. de Lamballerie, D. Malvy, A. Pizzorno, O. Terrier, M. Rosa Calatrava, F. Mentré, P. Smith, A. S. Perelson, J. Guedj, Timing of Antiviral Treatment Initiation is Critical to Reduce SARS-CoV-2 Viral Load. *CPT Pharmacometrics Syst Pharmacol* **9**, 509–514 (2020).

22. S. Iwanami, K. Ejima, K. Su Kim, K. Noshita, Y. Fujita, T. Miyazaki, S. Kohno, Y. Miyazaki, S. Morimoto, S. Nakaoka, Y. Koizumi, Y. Asai, K. Aihara, K. Watashi, R. N. Thompson, K. Shibuya, K. Fujiu, A. S. Perelson, S. Iwami, T. Wakita, Detection of significant antiviral drug effects on COVID-19 with reasonable sample sizes in randomized controlled trials: A modeling study. *PLoS Med* **18**, 25 (2021).

23. A. Goyal, E. F. Cardozo-Ojeda, J. T. Schiffer, Potency and timing of antiviral therapy as determinants of duration of SARS-CoV-2 shedding and intensity of inflammatory response. *Sci Adv* **6** (2020), doi:10.1126/sciadv.abc7112.
24. V. Fumagalli, P. Di Lucia, M. Ravà, D. Marotta, E. Bono, S. Grassi, L. Donnici, R. Cannalire, I. Stefanelli, A. Ferraro, F. Esposito, E. Pariani, D. Inverso, C. Montesano, S. Delbue, S. Perlman, E. Tramontano, R. De Francesco, V. Summa, L. G. Guidotti, M. Iannacone, Nirmatrelvir treatment of SARS-CoV-2-infected mice blunts antiviral adaptive immune responses. *EMBO Mol Med* **15**, e17580 (2023).
25. A. S. Perelson, R. M. Ribeiro, T. Phan, An explanation for SARS-CoV-2 rebound after Paxlovid treatment. *medRxiv* (2023), doi:10.1101/2023.05.30.23290747.
26. K. Owens, S. Esmaeili-Wellman, J. T. Schiffer, Heterogeneous SARS-CoV-2 kinetics due to variable timing and intensity of immune responses. *medRxiv* (2023), doi:10.1101/2023.08.20.23294350.
27. S. Galmiche, T. Cortier, T. Charmet, L. Schaeffer, O. Chény, C. Von Platen, A. Lévy, S. Martin, F. Omar, C. David, A. Mailles, F. Carrat, S. Cauchemez, A. Fontanet, SARS-CoV-2 incubation period across variants of concern, individual factors, and circumstances of infection in France: a case series analysis from the ComCor study. *Lancet Microbe* **4**, E409–E417 (2023).
28. C. L. Finch, J. Dyall, S. Xu, E. A. Nelson, E. Postnikova, J. Y. Liang, H. Zhou, L. E. DeWald, C. J. Thomas, A. Wang, X. Xu, E. Hughes, P. J. Morris, J. C. Mirsalis, L. H. Nguyen, M. P. Arolfo, B. Koci, M. R. Holbrook, L. E. Hensley, P. B. Jahrling, C. Schmaljohn, L. M. Johansen, G. G. Olinger, J. T. Schiffer, J. M. White, Formulation, Stability, Pharmacokinetic, and Modeling Studies for Tests of Synergistic Combinations of Orally Available Approved Drugs against Ebola Virus In Vivo. *Microorganisms* **9**, 566 (2021).
29. B. T. Mayer, A. C. deCamp, Y. Huang, J. T. Schiffer, R. Gottardo, P. B. Gilbert, D. B. Reeves, Optimizing clinical dosing of combination broadly neutralizing antibodies for HIV prevention. *PLoS Comput Biol* **18** (2022), doi:10.1371/JOURNAL.PCBI.1010003.
30. A. S. Anderson, P. Caubel, J. M. Rusnak, Nirmatrelvir–Ritonavir and Viral Load Rebound in Covid-19. *New England Journal of Medicine* **387**, 1047–1049 (2022).
31. G. E. Edelstein, J. Boucau, R. B. Uddin, C. B. Marino, M. Y. Liew BA, M. Barry, M. C. Choudhary, R. F. Gilbert, Z. Reynolds MPH, Y. Li, D. Tien BSA, S. B. Sagar, T. D. Vyas BS, Y. Kawano, J. A. Sparks MMsc, Z. Wallace, J. M. Vyas, J. E. Lemieux, J. Z. Li, M. J. Siedner, SARS-CoV-2 virologic rebound with nirmatrelvir-ritonavir therapy. , doi:10.1101/2023.06.23.23288598.
32. J. T. Schiffer, D. A. Swan, L. Corey, A. Wald, Rapid viral expansion and short drug half-life explain the incomplete effectiveness of current herpes simplex virus 2-directed antiviral agents. *Antimicrob Agents Chemother* **57**, 5820–5829 (2013).
33. D. B. Reeves, Y. Huang, E. R. Duke, B. T. Mayer, E. Fabian Cardozo-Ojeda, F. A. Boshier, D. A. Swan, M. Rolland, M. L. Robb, J. R. Mascola, M. S. Cohen, L. Corey, P. B. Gilbert, J. T. Schiffer, Mathematical modeling to reveal breakthrough mechanisms in the HIV Antibody Mediated Prevention (AMP) trials. *PLoS Comput Biol* **16** (2020), doi:10.1371/JOURNAL.PCBI.1007626.
34. J. T. Schiffer, D. A. Swan, A. Magaret, L. Corey, A. Wald, J. Ossig, H. Ruebsamen-Schaeff, S. Stoelben, B. Timmler, H. Zimmermann, M. R. Melhem, S. A. Van Wart, C. M. Rubino, A. Birkmann, Mathematical modeling of herpes simplex virus-2 suppression with pritelivir predicts trial outcomes. *Sci Transl Med* **8** (2016), doi:10.1126/SCITRANSLMED.AAD6654/SUPPL_FILE/AAD6654_VIDEO_S4.MOV.
35. S. R. Greenfield, H. Eng, Q. Yang, C. Guo, L. Byrnes, A. Dantonio, G. West, L. Di, A. S. Kalgutkar, Species differences in plasma protein binding of the severe acute respiratory syndrome coronavirus 2 (SARS-CoV-2) main protease inhibitor nirmatrelvir. *Xenobiotica* **53**, 12–24 (2023).
36. R. K. Hau, S. H. Wright, N. J. Cherrington, PF-07321332 (Nirmatrelvir) does not interact with human ENT1 or ENT2: Implications for COVID-19 patients. *Clin Transl Sci* **15**, 1599–1605 (2022).
37. G. E. Edelstein, J. Boucau, R. Uddin, C. Marino, M. Y. Liew, M. Barry, M. C. Choudhary, R. F. Gilbert, Z. Reynolds, Y. Li, D. Tien, S. Sagar, T. D. Vyas, Y. Kawano, J. A. Sparks, S. P. Hammond, Z. Wallace, J. M. Vyas, A. K. Barczak, J. E. Lemieux, J. Z. Li, M. J. Siedner, SARS-CoV-2 virologic rebound with nirmatrelvir-ritonavir therapy. *medRxiv* , 2023.06.23.23288598 (2023).
38. C. K. H. Wong, K. T. K. Lau, I. C. H. Au, E. H. Y. Lau, L. L. M. Poon, I. F. N. Hung, B. J. Cowling, G. M. Leung, Viral burden rebound in hospitalised patients with COVID-19 receiving oral antivirals in Hong Kong: a population-wide retrospective cohort study. *Lancet Infect Dis* **23**, 683–695 (2023).
39. J. A. Pandit, J. M. Radin, D. C. Chiang, E. G. Spencer, J. B. Pawelek, M. Diwan, L. Roumani, M. J. Mina, The Coronavirus Disease 2019 Rebound Study: A Prospective Cohort Study to Evaluate Viral and Symptom Rebound Differences in Participants Treated With Nirmatrelvir Plus Ritonavir Versus Untreated Controls. *Clin Infect Dis* **77** (2023), doi:10.1093/CID/CIAD102.
40. N. S. Zuckerman, E. Bucris, D. Keidar-Friedman, M. Amsalem, T. Brosh-Nissimov, Nirmatrelvir resistance-de novo E166V/L50V mutations in an immunocompromised patient treated with prolonged nirmatrelvir/ritonavir monotherapy leading to clinical and virological treatment failure-a case report. , doi:10.1093/cid/ciad494.
41. A. Jayk Bernal, M. M. Gomes da Silva, D. B. Musungaie, E. Kovalchuk, A. Gonzalez, V. Delos Reyes, A. Martín-Quirós, Y. Caraco, A. Williams-Diaz, M. L. Brown, J. Du, A. Pedley, C. Assaid, J. Strizki, J. A. Grobler,

H. H. Shamsuddin, R. Tipping, H. Wan, A. Paschke, J. R. Butterton, M. G. Johnson, C. De Anda, Molnupiravir for Oral Treatment of Covid-19 in Nonhospitalized Patients. *New England Journal of Medicine* **386**, 509–520 (2022).

42. K. M. Elias, S. R. Khan, E. Stadler, T. E. Schlub, D. Cromer, M. N. Polizzotto, S. J. Kent, T. Turner, M. P. Davenport, D. S. Khoury, Viral clearance as a surrogate of clinical efficacy for COVID-19 therapies in outpatients: A systematic review and meta-analysis. *medRxiv* , 2023.06.18.23291566 (2023).

43. R. L. Gottlieb, C. E. Vaca, R. Paredes, J. Mera, B. J. Webb, G. Perez, G. Oguchi, P. Ryan, B. U. Nielsen, M. Brown, A. Hidalgo, Y. Sachdeva, S. Mittal, O. Osiyemi, J. Skarbinski, K. Juneja, R. H. Hyland, A. Osinusi, S. Chen, G. Camus, M. Abdelghany, S. Davies, N. Behenna-Renton, F. Duff, F. M. Marty, M. J. Katz, A. A. Ginde, S. M. Brown, J. T. Schiffer, J. A. Hill, Early Remdesivir to Prevent Progression to Severe Covid-19 in Outpatients. *New England Journal of Medicine* **386**, 305–315 (2022).

44. A. F. Carlin, A. E. Clark, A. Chaillon, A. F. Garretson, W. Bray, M. Porrachia, A. L. T. Santos, T. M. Rana, D. M. Smith, Virologic and Immunologic Characterization of Coronavirus Disease 2019 Recrudescence After Nirmatrelvir/Ritonavir Treatment. *Clin Infect Dis* **76**, E530–E532 (2023).

45. B. P. Epling, J. M. Rocco, K. L. Boswell, E. Laidlaw, F. Galindo, A. Kellogg, S. Das, A. Roder, E. Ghedin, A. Kreitman, R. L. Dewar, S. E. M. Kelly, H. Kalish, T. Rehman, J. Highbarger, A. Rupert, G. Kocher, M. R. Holbrook, A. Lisco, M. Manion, R. A. Koup, I. Sereti, Clinical, Virologic, and Immunologic Evaluation of Symptomatic Coronavirus Disease 2019 Rebound Following Nirmatrelvir/Ritonavir Treatment. *Clin Infect Dis* **76**, 573–581 (2023).

46. J. Boucau, R. Uddin, C. Marino, J. Regan, J. P. Flynn, M. C. Choudhary, G. Chen, A. M. Stuckwisch, J. Mathews, M. Y. Liew, A. Singh, Z. Reynolds, S. L. Iyer, G. C. Chamberlin, T. D. Vyas, J. M. Vyas, S. E. Turbett, J. Z. Li, J. E. Lemieux, A. K. Barczak, M. J. Siedner, Characterization of Virologic Rebound Following Nirmatrelvir-Ritonavir Treatment for Coronavirus Disease 2019 (COVID-19). *Clin Infect Dis* **76**, E526–E529 (2023).

47. C. C. Lai, P. R. Hsueh, Coronavirus disease 2019 rebounds following nirmatrelvir/ritonavir treatment. *J Med Virol* **95** (2023), doi:10.1002/JMV.28430.

48. J. A. Hay, S. M. Kissler, J. R. Fauver, C. Mack, C. G. Tai, R. M. Samant, S. Connolly, D. J. Anderson, G. Khullar, M. Mackay, M. Patel, S. Kelly, A. Manhertz, I. Eiter, D. Salgado, T. Baker, B. Howard, J. T. Dudley, C. E. Mason, M. Nair, Y. Huang, J. Difiori, D. D. Ho, N. D. Grubaugh, Y. H. Grad, Quantifying the impact of immune history and variant on SARS-CoV-2 viral kinetics and infection rebound: A retrospective cohort study. *Elife* **11** (2022), doi:10.7554/eLife.81849.

49. R. S. P. Singh, S. S. Toussi, F. Hackman, P. L. Chan, R. Rao, R. Allen, L. Van Eyck, S. Pawlak, E. P. Kadar, F. Clark, H. Shi, A. S. Anderson, M. Binks, S. Menon, G. Nucci, A. Bergman, Innovative Randomized Phase I Study and Dosing Regimen Selection to Accelerate and Inform Pivotal COVID-19 Trial of Nirmatrelvir. *Clin Pharmacol Ther* **112**, 101–111 (2022).

50. D. R. Owen, C. M. N. Allerton, A. S. Anderson, L. Aschenbrenner, M. Avery, S. Berritt, B. Boras, R. D. Cardin, A. Carlo, K. J. Coffman, A. Dantonio, L. Di, H. Eng, R. A. Ferre, K. S. Gajiwala, S. A. Gibson, S. E. Greasley, B. L. Hurst, E. P. Kadar, A. S. Kalgutkar, J. C. Lee, J. Lee, W. Liu, S. W. Mason, S. Noell, J. J. Novak, R. S. Obach, K. Ogilvie, N. C. Patel, M. Pettersson, D. K. Rai, M. R. Reese, M. F. Sammons, J. G. Sathish, R. S. P. Singh, C. M. Steppan, A. E. Stewart, J. B. Tuttle, L. Updyke, P. R. Verhoest, L. Wei, Q. Yang, Y. Zhu, An oral SARS-CoV-2 Mpro inhibitor clinical candidate for the treatment of COVID-19. *Science* **374**, 1586–1593 (2021).

51. J. Wagoner, S. Herring, T.-Y. Hsiang, A. Ianevski, S. B. Biering, S. Xu, M. Hoffmann, S. Pöhlmann, M. Gale, T. Aittokallio, J. T. Schiffer, J. M. White, S. J. Polyak, Combinations of Host- and Virus-Targeting Antiviral Drugs Confer Synergistic Suppression of SARS-CoV-2. *Microbiol Spectr* **10** (2022), doi:10.1128/SPECTRUM.03331-22.

Acknowledgments

Funding:

National Institutes of Health (NIH) grants R01AI169427 (JTS)

National Institutes of Health (NIH) grants R01AI121129 (JTS)

National Institutes of Health (NIH) grants R01AI177512 (JTS, SJP)

Author contributions:

Conceptualization: JTS, SE, KO
Methodology: JTS, SE, KO
Software: SE, KO
Investigation: SJP, JW, SE, KO
Formal analysis: SE, KO
Writing – original draft: JTS, SE
Writing – review & editing: JTS, SE, KO, SJP, JW, JMW

Competing interests:

Authors declare that they have no competing interests.

Data and materials availability:

All code, and materials used in the analysis is available on github at https://github.com/sEsmaeili/Covid_Rebound

The data analyzed in this work was previously published by Hay et al. and Schilling et al. and is available on github at https://github.com/gradlab/SC2-kinetics-immune-history and https://github.com/jwatowatson/PLATCOV-Molnupiravir/tree/V1.0

Figures and Tables

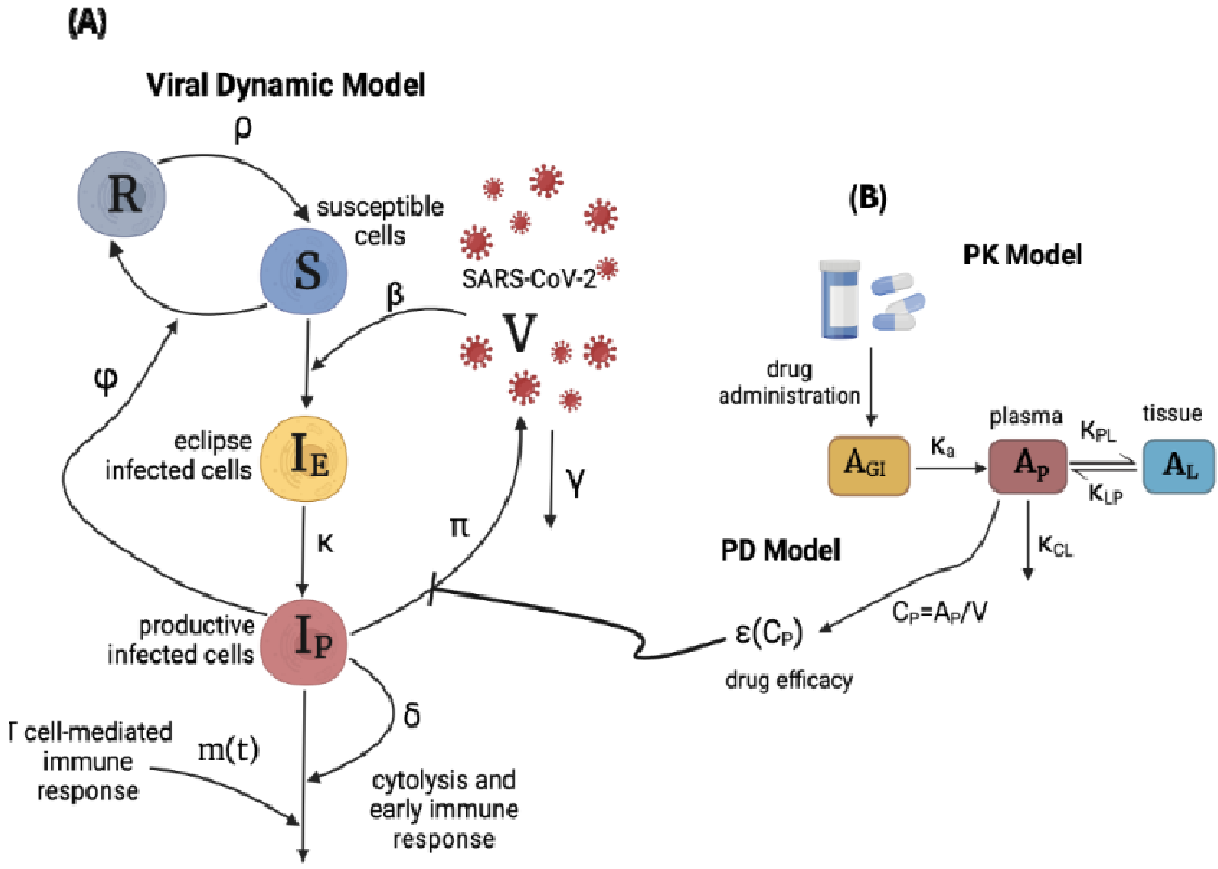

Fig. 1. Schematics of the viral dynamic model and nirmatrelvir PK-PD two compartmental model. (A) The viral dynamic model follows the dynamics of susceptible cells (S), refractory cells (R), eclipse infected cells (I_E), productively infected cells (I_P), and virus (V) and includes the early and late cytolytic T-cell immune responses with rates and m(t). is the infection rate, is the rate of reversion of refractory cells to susceptible cells. Infected cells produce viruses at the rate , and the free viruses are cleared at the rate . **(B)** Two-compartmental PK model with oral administration of the drug which models the amounts of the drug in gut tissue (A_{GI}), plasma (A_P), and the tissue (A_L). K_a is the rate of absorption of the drug from gut to plasma. K_{PL} and K_{LP} are the rates of transfer of the drug from plasma to the tissue and back, and K_{CL} is the rate at which the drug clears from the body. V is the estimated plasma volume and C_P is the drug concentration in plasma. is the drug efficacy that blocks viral production and is calculated using the Hill equation: ———— where Emax is the maximum efficacy, n is the Hill coefficient, IC50 is the concentration of drug *in vitro* at which viral replication rate is reduced by 50%, prf is the potency reduction factor translating the *in vitro* potency to *in vivo* potency.

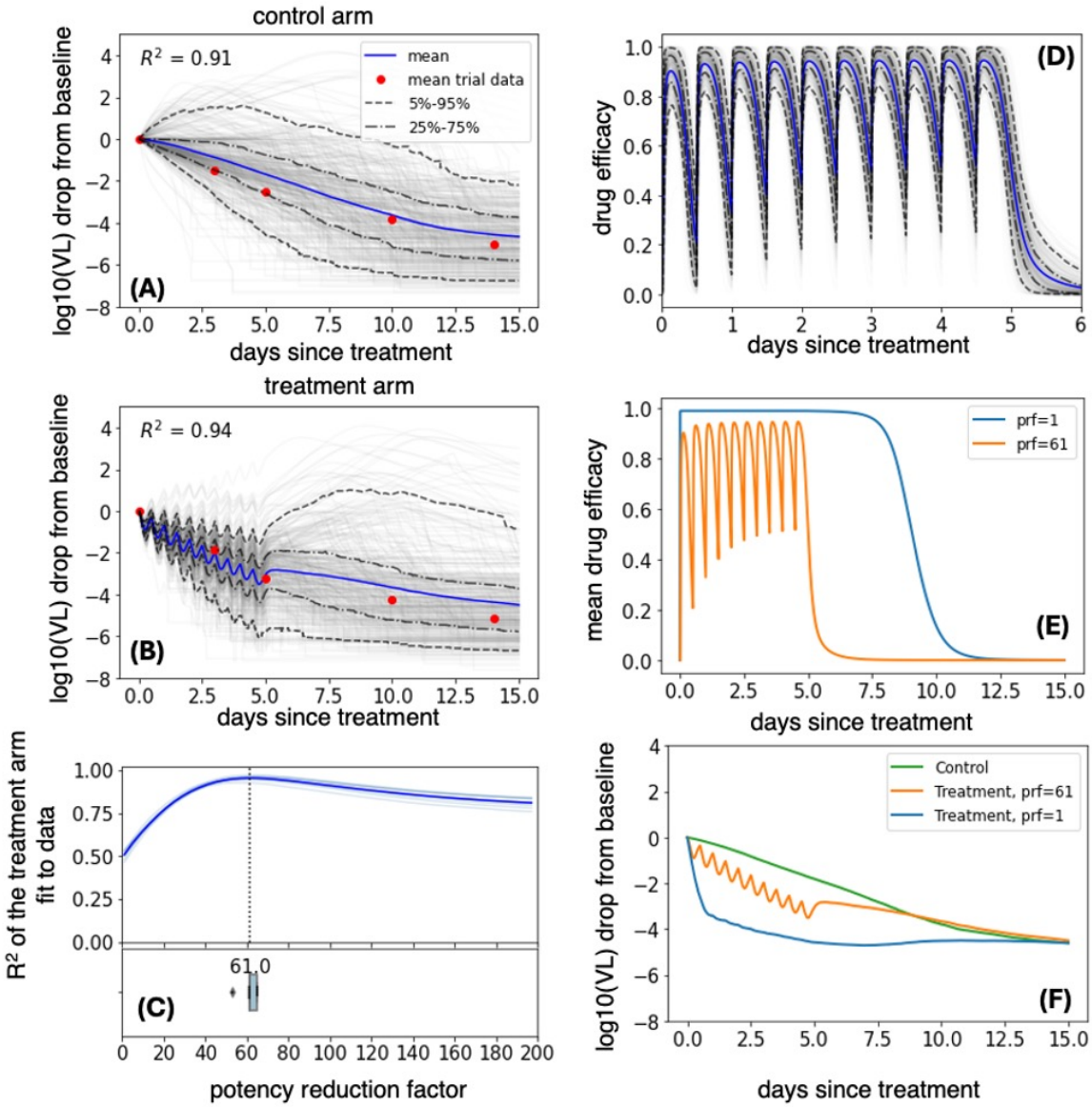

Fig. 2. Lower *in vivo* potency of nirmatrelvir relative to *in vitro* potency in EPIC-HR. (A-B) mean (blue), individual (gray), and ranges (labeled dashed lines) of log10 viral load drop from the baseline of individuals randomly selected from the NBA cohort treated with **(A)** placebo or **(B)** five days of nirmatrelvir / ritonavir 300 mg twice daily. The red dots were obtained by digitizing Fig 3a of Hammond et al.*(1)* and model fit was noted by closeness of blue lines to the red dots. **(C)** R^2 of the fit of the 10 model simulations per prf to the viral load drop data in light blue and their mean in dark blue. The best model fit was at a potency reduction factor of 61. The horizontal boxplot in the lower panel shows the distribution of prf values at which R^2 is maximum (mean = 61.8, median =61, sd=3.5). **(D)** Drug efficacy when prf=61. Average efficacy was 82% over the 5-day interval, with notable drops in antiviral efficacy at drug troughs. **(E)** Average drug efficacy when prf = 1 vs prf = 61. The drug with no potency reduction has nearly perfect efficacy (average efficacy of 99.99%) over 5 days and has a prolonged post-treatment effect. **(F)** mean log10 viral load drop from baseline of the control arm, treatment arm with prf=61, and treatment arm with prf=1.

887

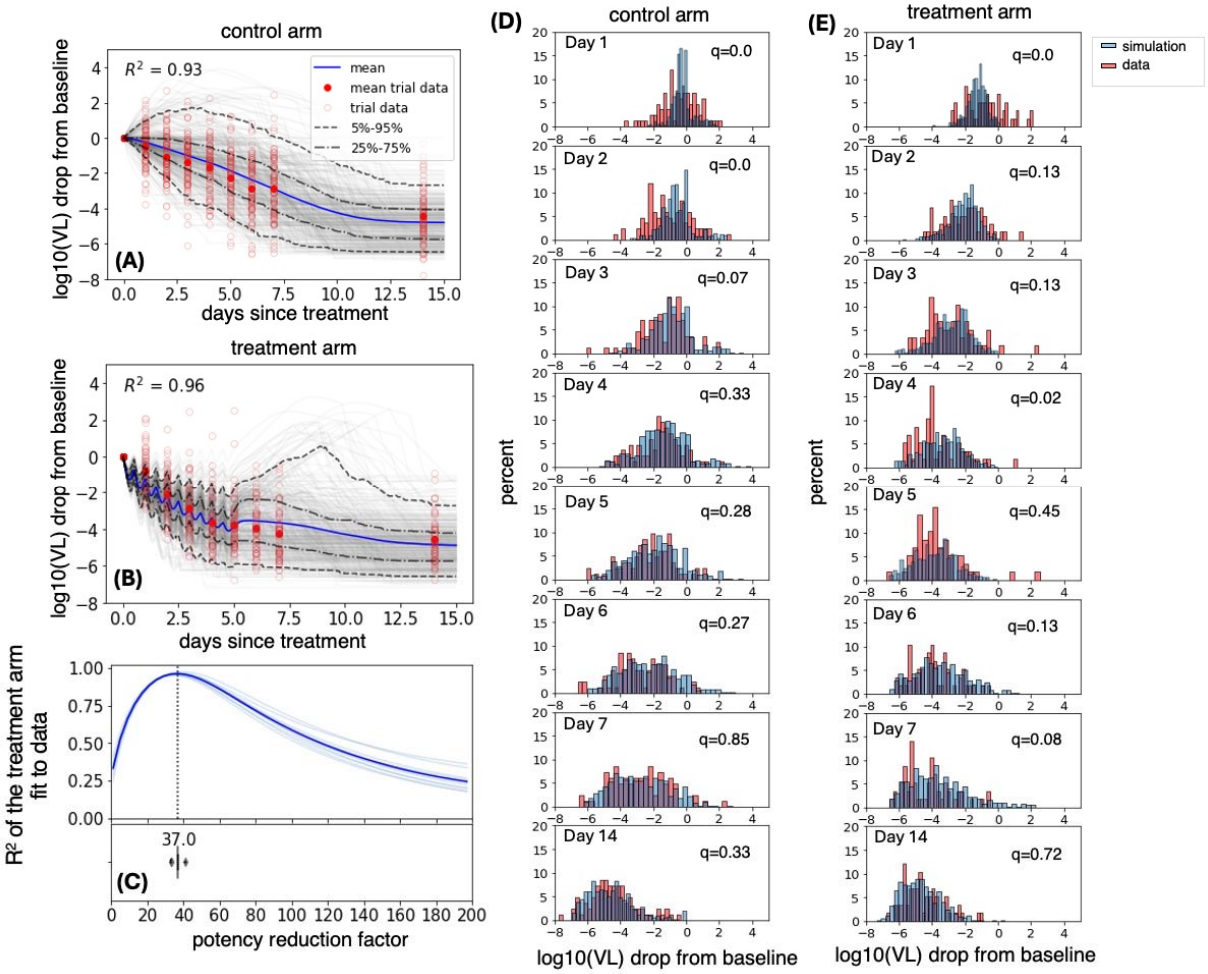

888
889

890 **Fig. 3. Lower *in vivo* potency of nirmatrelvir relative to *in vitro* potency in**
891 **PLATCOV. (A-B)** mean (blue), individual (gray), and ranges (labeled dashed
892 lines) of log10 viral load drop from the baseline of individuals randomly
893 selected from the NBA cohort treated with **(A)** placebo or **(B)** five days of
894 nirmatrelvir / ritonavir 300 mg twice daily. The empty and filled red circles are
895 individual and mean viral load drop from baseline calculated from viral load
896 data published by Schilling et al.*(5)*. Model fit was noted by closeness of blue
897 lines to the filled red dots. **(C)** R^2 of the fit of the 10 model simulations per prf
898 to the viral load drop data in light blue and their mean in dark blue. The best
899 model fit was at a potency reduction factor of 37. The horizontal boxplot in the
900 lower panel shows the distribution of prf values at which R^2 is maximum (mean
901 = 36.6, median =37, sd=2.15). **(D-E)** distribution of log10 viral load drop from
902 baseline of simulated cohort and the 144 individuals in PLATCOV control arm
903 **(D)** and treatment arm **(E)**. Adjusted p-values (q-values) were calculated using
904 Benjamini-Hochberg method and represent dissimilarity between observed and
905 simulated distributions.

906

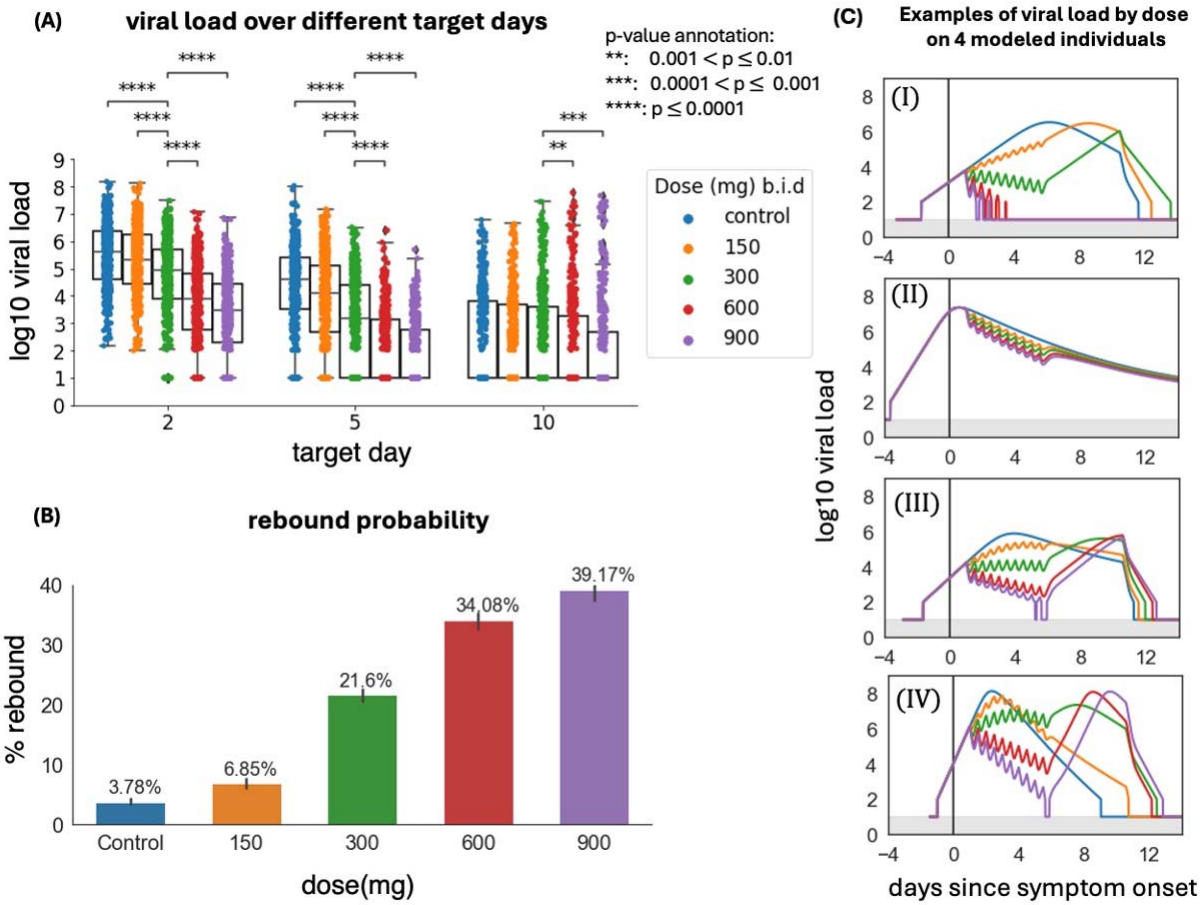

Fig. 4. Increasing nirmatrelvir dose lowers short term viral load but increases probability of viral rebound. In all scenarios, simulated treatment starts within the first 3 days post-symptoms. **(A)** log10 viral load at days 2, 5, and 10 after the treatment start day with different doses. p-values were obtained by performing Mann-Whitney U-test between the 300 mg group and the others, and only p-values <0.01 are shown. Viral loads were only reduced by higher doses at days 2 and 5, but not day 10. **(B)** The probability of rebound for different doses. The error bars on each column are 95% confidence intervals. **(C)** Examples of viral load trajectories assuming different doses on 4 modeled individuals with equivalent timing of therapy and untreated viral kinetics.

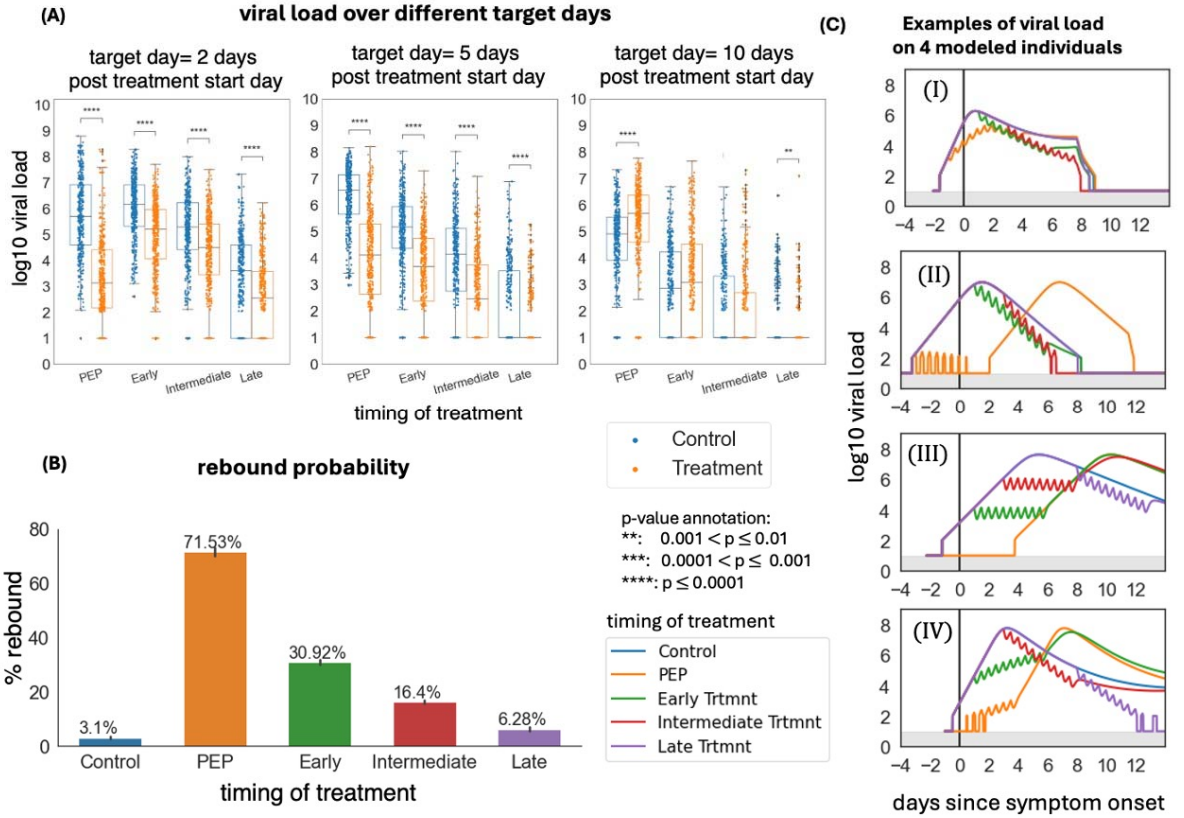

Fig. 5. Early timing of therapy initiation is a key risk factor for viral rebound. In all simulations, the dose was 300 mg twice daily for five days. **(A)** log10 viral load at days 2, 5, and 10 after the treatment start day with different treatment durations. p-values were obtained by performing Mann-Whitney U-test. At day 10, the treatment group had higher viral loads compared to placebo due to viral rebound in the PEP and early treatment simulations, despite lowering viral loads significantly at days 2 and 5. **(B)** The probability of rebound for different treatment timing. The error bars on each column are 95% confidence interval **(C)** Samples of viral load trajectories assuming different treatment timing on 4 modeled individuals with equivalent untreated viral kinetics.

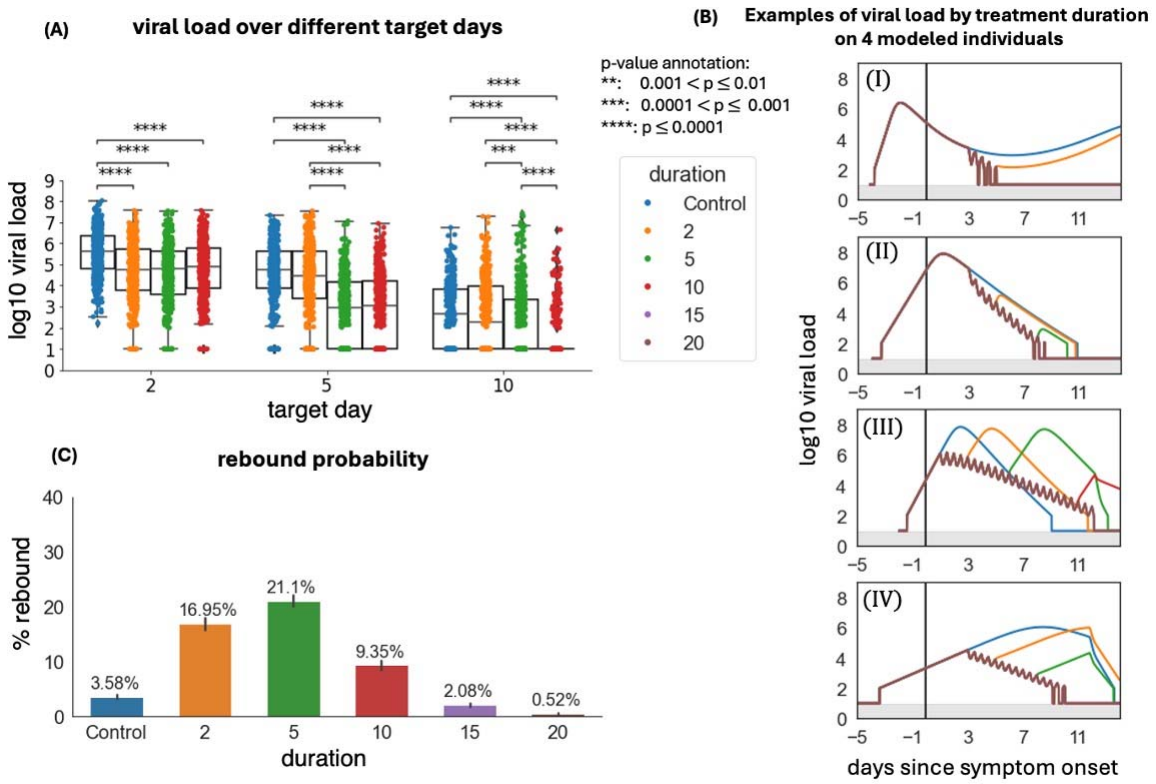

Fig. 6. Prolonging treatment duration limits rebound probability. In all simulations, treatment starts within the first 3 days post-symptoms and the dose was 300 mg twice daily. **(A)** log10 viral load at days 2, 5, and 10 after the treatment start day with different treatment durations. p-values were obtained by performing Mann-Whitney U-test and only values <0.01 are shown. At day 10, the control group had equivalent viral loads to 5 days of treatment while 10 days of treatment significantly lowered viral load. **(B)** The probability of rebound for different treatment durations. The error bars on each column are 95% confidence interval.**(C)** Samples of viral load trajectories assuming different treatment durations on 4 modeled individuals with equivalent timing of therapy and untreated viral kinetics. Prolonging therapy often avoids rebound.

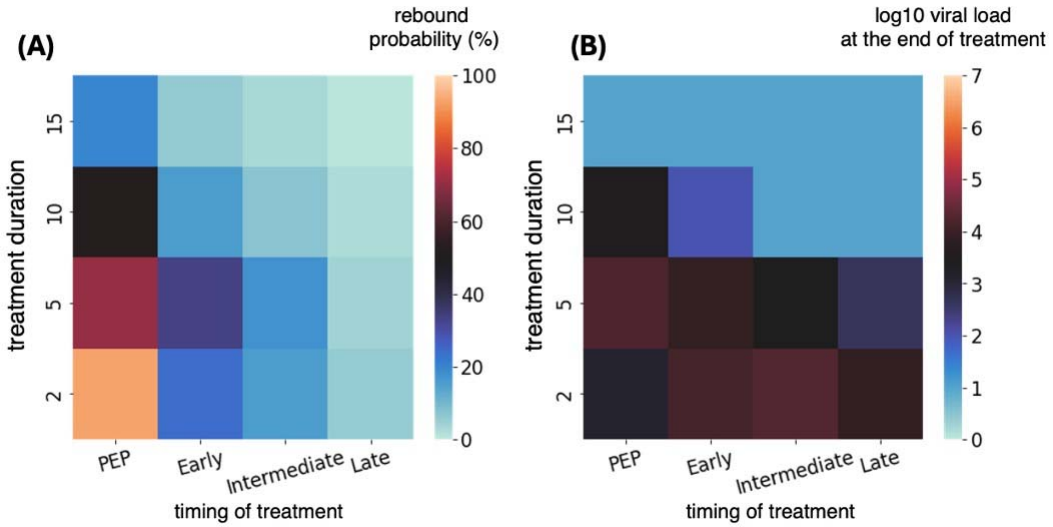

Fig. 7. Post-exposure prophylaxis requires more prolonged therapy than early symptomatic therapy to avoid viral rebound. (A) probability of rebound and **(B)** viral load at the end of the treatment as a function of treatment timing and duration.

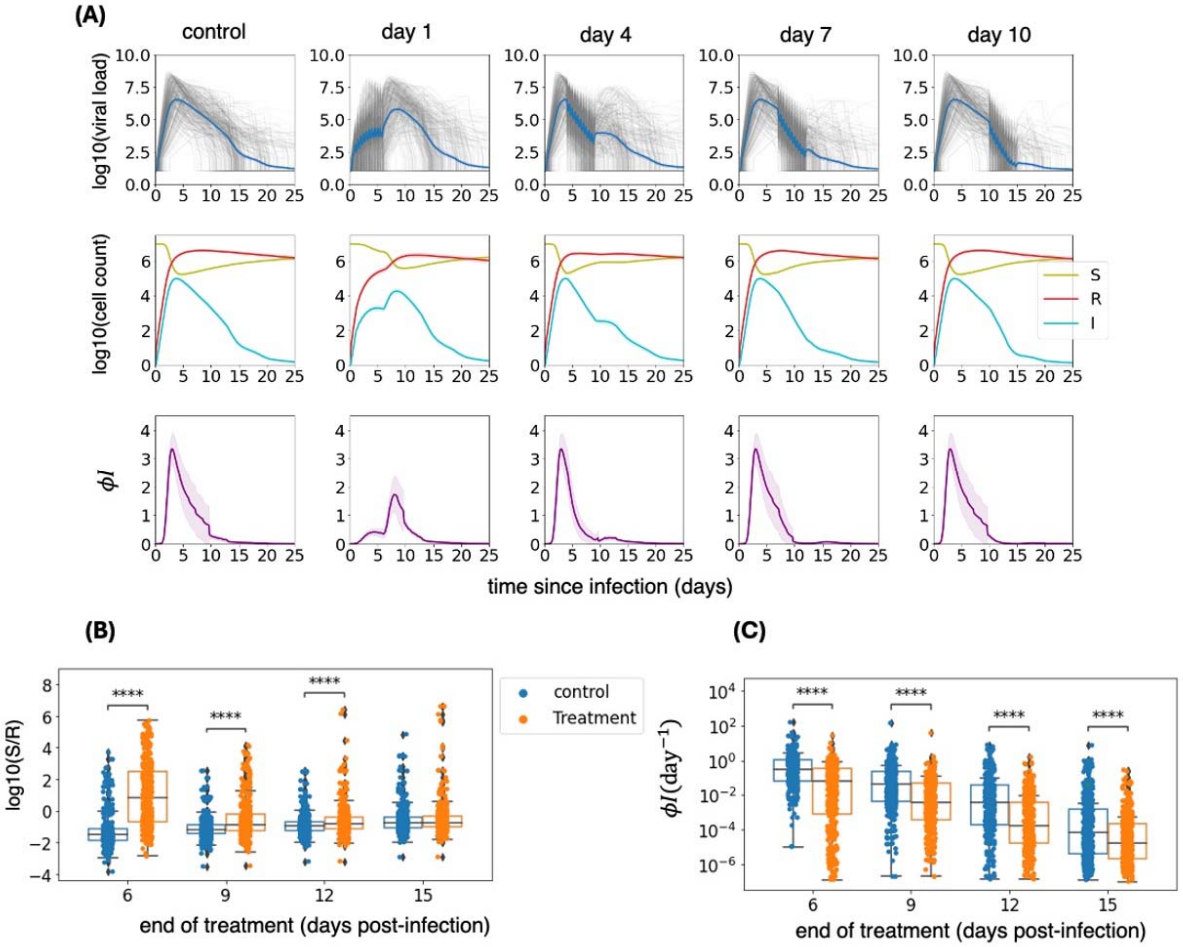

Fig. 8. Early therapy preserves susceptible cells, limits refractory cells, does not eliminate all infected cells, and delays innate immune responses. Simulations are performed using time since infection as a variable rather than based on symptoms as in prior figures to eliminate the confounding impact of variable incubation period. **(A)** The top row shows the viral load of all individuals (in grey) and the average viral load (in blue). The middle row shows a less substantial depletion of susceptible cells (S), and lower generation of refractory cells (R) with earlier therapy. The bottom row shows the rate of production of refractory cells likely representing innate immune responses per day with biphasic, lower peak responses noted with early therapy and to a lesser extent in day 4 treated individuals. **(B)** Ratios of susceptible (S) to refractory cells (R) at the end of the 5-day treatment for different timings of treatment. **(C)** Per cell production rate of refractory cells at the end of the 5-day treatment for different timings of treatment.